Compensation of Unbalance Forces of a Switched Reluctance Machine with Combined Current and Fluxlinkage Control

Thomas Hinterdorfer, Alexander Schulz, Harald Sima, Stefan Hartl and Johann Wassermann

Vienna University of Technology, Institute of Mechanics and Mechatronics,
Wiedner Hauptstraße 8-10, A-1040 Vienna, Austria,
{givenname.surname}@tuwien.ac.at

Abstract—The presented work handles the compensation of unbalance forces for a 6/4-Switched Reluctance Machine (SRM), which generate significant radial magnetic forces in an eccentric motor shaft position. When the rotor is operating e.g. in its principal axis of inertia, these forces must be compensated by the bearings. This is of major interest for long term storage Flyweels where bearing efficiency is a key factor for the overall system performance.

Due to the back electromotive force (BEMF) in high speed operation, precise current control is a major challenge. Hence a combination of current and fluxlinkage control is used to minimize the generated radial forces. It can be used for low and high speed applications.

For the observation of fluxlinkage two different methods are described. The functionallity is shown by means of simulations and measurement.

I. Introduction

Flywheel Energy Storage Systems (FESS) represent an ecologically and economically sustainable technology for decentralized energy storage. Compared to other storage technologies such as e.g. accumulators, they offer longer life cycles without performance degradation over time and usage and need almost no systematic maintenance. To achieve a high energy density FESS rotors are usually manufactured of fiber reinforced plastics, which enables tip speeds up to 800 m/s.

For long term storage Flywheel applications magnetic bearings for rotor support are used and the rotor is operated in an evacuated containment to minimize drag. Due to losses in coils, iron, electronics and air drag the self-discharge is usually rather high. The bearings are optimized with respect to efficiency to maximize storage time.

The stator and the rotor of a SRM have salient poles, see Fig. 1, where the geometry of a 6/4-SRM is shown. Hence, the airgap changes with the rotor angle θ. When a phase, consisting of two opposing coils, is excited, the rotor attempts to align with the stator to minimize reluctance. Thus, by sequentially exciting the machines phases, a continuous rotation can be achieved. The SRM has no permanent magnets in its assembly and therefore minimal holding torque. Furthermore, the rotor mass and its moment of inertia is rather small refered to its torque. These are essential advantages for long term storage Flywheels. The machines disadvantages are
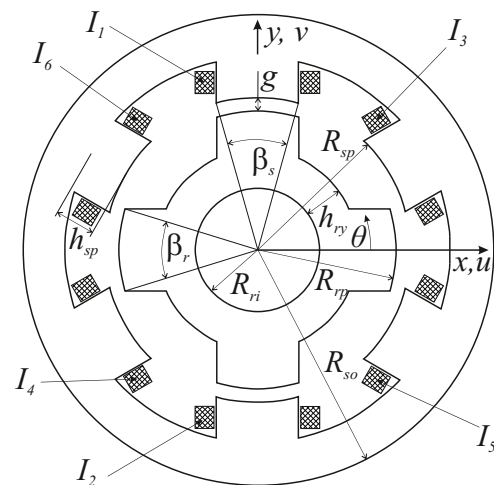

Figure 1. Definitions and geometry of the examined machine in aligned position with the rotor angle $\theta = 0°$

high torque ripple and a complex control due to the nonlinear behaviour. Furthermore the SRM requires an electronic power converter to run.

To maximize efficiency of the radial magnetic bearings the rotor is held in its principle axis of inertia by unbalance control, to cancel out speed synchronous currents and consequently provide a minimum of energy for radial support. Hence, the machine's operating point will be in an eccentric position. Moreover, the high tip speed causes large rotor deformations leading to an unbalance which depends on the angular velocity. When the rotor of an SRM is in an eccentric position radial forces are generated due to different reluctances of the two opposing airgaps. This forces must be compensated again by the magnetic bearings and therefore decreasing there efficiency. Thereby the concept presented in this paper is to control the two coils of a SRM-phase separately, with the goal of generating no resulting forces and thereby minimizing the influence of the machine on the magnetic bearings. Furthermore the presented concept also enables a bearingless operation of the machine, which increases the reliability of a FESS and allows a smaller design of the bearings.

Compensation methods for unbalanced synchronous- and

induction machines are described e.g. in [1], where connecting the phase coils in parallel is leading to a balanced fluxlinkage. An analogous method is described in [2] and [3], where the unbalance forces of a three phase 12/8-SRM are compensated. In that paper only machine topologies with four coils or more in one phase are investigated. It was shown that two parallel branches with neighboring coils in series and opposing coils in parallel and an equalizer between them is leading to the best compensation.

[4] discusses the effect of short circuited coils on the rotor which avoids an asymmetric flux distribution. The advantage of this method is, that no additional power converters are necessary, but it results in an increased constructional effort.

In [5] the compensation is done by adjusting the ampere turns of the phase. The number of turns of the stator coils can be increased or decreased by switches. The change of torque is adjusted by the amplitude of the current. The disadvantage of this method is that the number of turns can only be changed in discrete steps. The required correction is dependent on the actual eccentricity and can be detected by mutual coupling which is described in [6].

[7] uses an analytical function to determine the reference current for force compensation, which are dependent on the rotor angle and the displacement. A 12/8-SRM is described and the compensation method is to control the current of opposing coils separately.

II. OVERVIEW

SRMs generate high magnetic forces in an eccentric run. Therefore in the following a comepensation method will be presented. Chapter III deals with a current controlled machine to achieve the required power in combination with a fluxlinkage controller to compensate unbalance forces. For this purpose two different fluxlinkage observers will be discussed. In chapter IV the used model will be presented which then will be compared to measurement data discussed in chapter VI done at the test rig presented in chapter V. Finally chapter VII concludes the paper.

The data of the examined machine with a nominal power of 5 kW and an operating range of 650 rad/s to 2000 rad/s are summarized in Table I and the definitions are shown in Fig. 1.

In the following mutual coupling of the phases is neglected and only one phase with coils 1 and 2 is considered.

III. COMPENSATION OF UNBALANCE FORCES

To compensate unbalance forces and enable a bearingless operation, the two opposing coils of one phase are controlled separately. A block diagram of the control scheme is shown in Fig. 2. To achieve the needed torque or power a superior controller generates firing angles and a reference current I_{cmd} for a current controller, which calculates the needed normalized voltage as an input for a pulse-width-modulator

$$d_{cmd,1,2} = \frac{1}{U_{DC}} \left(K_{P,I} L(\theta) \left(I_{cmd} - I_{1,2} \right) + \underbrace{\frac{dL(\theta)}{d\theta} I_{1,2} \omega}_{\text{BEMF}} \right) \quad (1)$$

Table I
DATA OF THE EXAMINED SRM

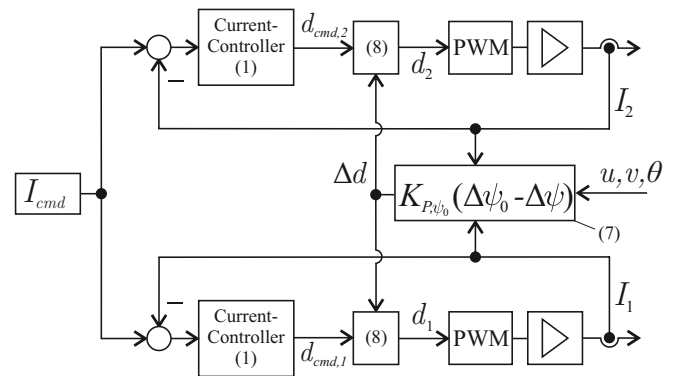|		
number stator poles	P_s	6
number rotor poles	P_r	4
rotor pole angle, °	β_r	38
stator pole angle, °	β_s	37
shaft radius, mm	R_{ri}	45.88
rotor pole radius, mm	R_{rp}	79
rotor yoke thickness, mm	h_{ry}	25.38
stator pole height, mm	h_{sp}	24.13
stator pole radius, mm	R_{sp}	80
stator outer radius, mm	R_{so}	139.7
stack length, mm	L_s	67.99
airgap length, mm	g	1
turns per coil	N	80

Figure 2. Block diagram of the control scheme

with the link voltage U_{DC}, the overall inductance in centered position L, the actual current $I_{1,2}$ in coil 1 or 2 and the angular velocity ω. A proportional controller with $K_{P,I}$ as gain and feedforward control of the BEMF is used. $K_{P,I}$ can be a function of ω to enable more flexibility.

A. Control Scheme

In case of an eccentric run, the concept of the presented controller is to use the current controller in (1) for the coil which has the larger airgap. In the coil with the smaller airgap the normalized voltage is decreased to adapt the fluxlinkage to achieve vanishing forces. The acting forces and the fluxlinkages can be determined by a magnetic circuit model or a finite element model as e.g. in [8]. When a positive displacement v in y-direction is assumed, the current in coil 2 can be controlled to the reference value and the current in coil 1 must be decreased. The difference of the two fluxlinkages of coil 1 and 2 can be derived by solving for vanishing force in y-direction at constant rotor angle θ, excitation current I_2 as well as translatory displacements u and v

$$F_y(\theta, I_1 = I_{cmd} - \Delta I_0, I_2 = I_{cmd}, u, v) = 0 \quad . \quad (2)$$

This results in a current difference ΔI_0 which can be substituted into the fluxlinkages, leading to the reference value of
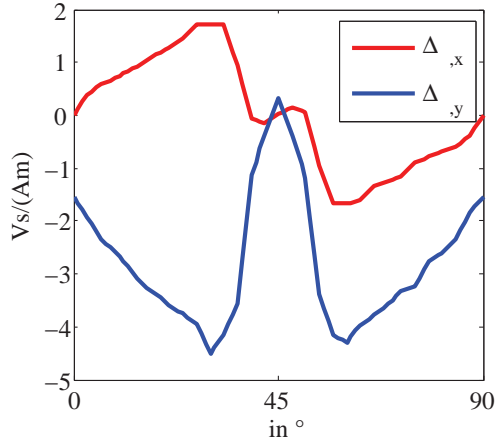
Figure 3. Fluxlinkage correction due to displacement u and v

the fluxlinkage difference

$$\Delta\psi_0 = \psi_1 - \psi_2 \qquad (3)$$

which is also a funtion of the rotor position and the excitation currents. When linear material behaviour is assumed, $\Delta\psi_0$ variies linear with the current. Due to increasing BEMF with higher angular velocity the actual current won't match the reference so the actual current is used to form the reference of the fluxlinkage difference

$$\Delta\psi_0 = \begin{cases} \Psi_0(\theta, u, v) I_1 & \text{for} \quad \Psi_0 > 0 \\ \Psi_0(\theta, u, v) I_2 & \text{for} \quad \Psi_0 \le 0 \end{cases} . \qquad (4)$$

Furthermore the superposition principle can be used and Ψ_0 can be written as a linear combination of u and v

$$\Psi_0(\theta, u, v) = \Delta_{\psi,x}(\theta) u + \Delta_{\psi,y}(\theta) v \qquad (5)$$

with the fluxlinkage correction $\Delta_{\psi,x}$ and $\Delta_{\psi,y}$, which can be seen in Fig. 3, due to displacements u and v, respectively. Due to Faraday's law of induction

$$d_{1,2} = \frac{U_{1,2}}{U_{DC}} = \frac{1}{U_{DC}} \frac{d\psi_{1,2}}{dt} \qquad (6)$$

the fluxlinkage can be adjusted by a voltage correction Δd which can be done by a proportional controller

$$\Delta d = K_{P,\psi_0} (\Delta\psi_0 - \Delta\psi) \qquad (7)$$

with d_1 and d_2 as the normalized voltages of the two coils, the applied voltages U_1 and U_2, the controller gain K_{P,ψ_0} and the actual fluxlinkage $\Delta\psi$.

To prevent overcurrent a distinction of cases is advantageous

$$\begin{aligned} \left. \begin{aligned} d_2 &= d_{cmd,2} \\ d_1 &= d_2 - \Delta d \end{aligned} \right\} &\quad \text{for} \quad \Delta\psi_0 \le 0 \\ \left. \begin{aligned} d_1 &= d_{cmd,1} \\ d_2 &= d_1 + \Delta d \end{aligned} \right\} &\quad \text{for} \quad \Delta\psi_0 > 0 \end{aligned} . \qquad (8)$$

In case of negative $\Delta\psi_0$, which arises for a positive displacement v the voltage correction is subtracted from d_1, and for a

positive value it is added to d_2. This procedure should prevent overcurrent and is not sensitive to noise in comparison to the usage of Δd for the distinction in (8).

B. Fluxlinkage Observer

In (7) the actual fluxlinkage difference is needed which can hardly be measured, hence an observer will be used. One method is to directly use the differential equation

$$\begin{aligned} \Delta\psi &= \psi_1 - \psi_2 \\ &= \int_0^t \left[U_{DC}(d_1 - d_2) - R(I_2 - I_1) \right] dt \end{aligned} \qquad (9)$$

with the ohmic resistance R. Transformation into discrete time domain leads to

$$\Delta\psi = \Delta\psi z^{-1} + T_s \left[U_{DC}(d_1 - d_2) + R(I_2 - I_1) \right] \qquad (10)$$

with the sampling time T_s. This kind of observer is very accurate at high speeds and when the current drops to zero after excitation. Otherwise a measurement or sampling error will be summed up due to the integral behaviour. Especially at low speeds this leads to instabilities due to the large excitation time span and therefore to high radial forces. For this reason this observer won't be considered in chapter VI.

Another method is to use the definition of secant inductance

$$\psi_1 = L_{11}(\theta, u, v) I_1 + L_{12}(\theta, u, v) I_2 \qquad (11)$$

with the self-inductance L_{11} and the mutual inductance L_{12} which are both functions of the rotor position. For small displacements u and v, i.e. in the linear part of the magnetization curve, the fluxlinkage of coil 1 can be linearized around the geometric center as follows

$$\psi_1 \approx \left[L_{11}(\theta)\big|_0 + \frac{\partial L_{11}(\theta)}{\partial x}\bigg|_0 u + \frac{\partial L_{11}(\theta)}{\partial y}\bigg|_0 v \right] I_1 + ... \\ \left[L_{12}(\theta)\big|_0 + \frac{\partial L_{12}(\theta)}{\partial x}\bigg|_0 u + \frac{\partial L_{12}(\theta)}{\partial y}\bigg|_0 v \right] I_2 . \qquad (12)$$

Due to symmetry the relations for ψ_2 are similar

$$\begin{aligned} L_{22}(\theta)\big|_0 &= L_{11}(\theta)\big|_0 &&= L_{11,0} \\ L_{21}(\theta)\big|_0 &= L_{12}(\theta)\big|_0 &&= L_{12,0} \\ \frac{\partial L_{11}(\theta)}{\partial x}\bigg|_0 &= -\frac{\partial L_{22}(\theta)}{\partial x}\bigg|_0 &&= L_{11,x0} \\ \frac{\partial L_{12}(\theta)}{\partial x}\bigg|_0 &= -\frac{\partial L_{21}(\theta)}{\partial x}\bigg|_0 &&= L_{12,x0} \\ \frac{\partial L_{11}(\theta)}{\partial y}\bigg|_0 &= -\frac{\partial L_{22}(\theta)}{\partial y}\bigg|_0 &&= L_{11,y0} \\ \frac{\partial L_{12}(\theta)}{\partial y}\bigg|_0 &= -\frac{\partial L_{21}(\theta)}{\partial y}\bigg|_0 &&= L_{12,y0} \end{aligned} \qquad (13)$$
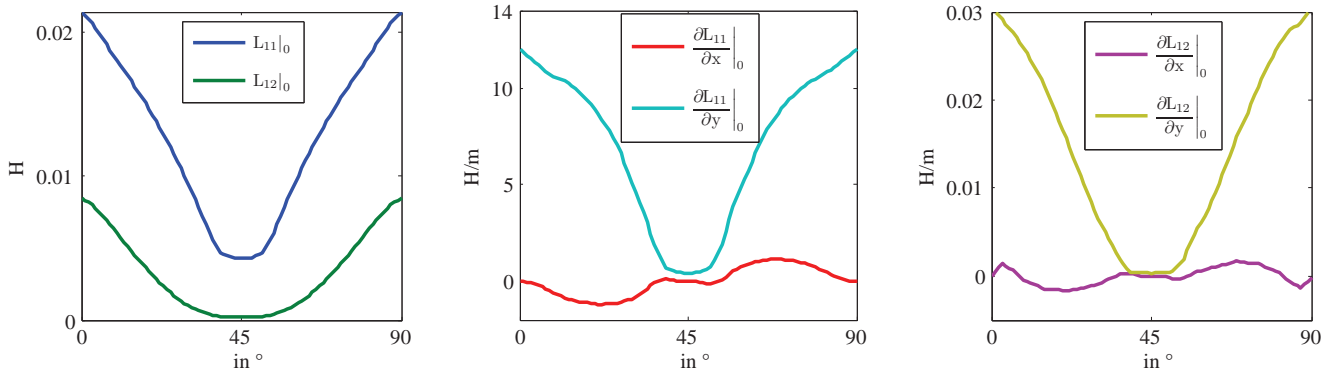
Figure 4. Self-inductance and mutual inductance (left); Derivative of self-inductance with respect to x and y (middle); Derivative of mutual inductance with respect to x and y (right)

and the fluxlinkage difference is derived as

$$\Delta \psi = (L_{11,0} - L_{12,0})(I_1 - I_2) + ...$$
$$\left[(L_{11,x0} + L_{12,x0}) u + ... \right.$$
$$\left. (L_{11,y0} + L_{12,y0}) v \right] (I_1 + I_2) \quad (14)$$

which now has low computational effort. The self- and mutual inductance as well as their derivatives are shown in Fig. 4. The fluxlinkages can be determined by three look-up tables which are only a function of the rotor angle and therefor can be calculated online with low requirement on memory.

IV. SIMULATION MODEL

For an accurate analysis of the machines behaviour, a detailed model was built. It contains the machines characteristics in look-up-tables determined by a 2D finite element analysis containing a nonlinear material description, described in [8], therefore end-effects were neglected. The characterestics of torque, forces and the fluxlinkages depend on the rotor position and the excitation currents. The fluxlinkages are unique functions of the currents, therefore they can be converted into each other and the integral form of (6) can be used for simulation

$$\psi_1 = \int_0^t \left[U_1 - RI_1(\theta, \psi_1, I_2, u, v) \right] dt$$
$$\psi_2 = \int_0^t \left[U_2 - RI_2(\theta, I_1, \psi_2, u, v) \right] dt \quad . \quad (15)$$

The model also includes noise of the current sensor, which was assumed to be triangular with an amplitude of 0.4 A at a frequency of 475 kHz. Before converting the signals into the digital domain by analog-to-digital converters (ADC) the current signal is fed through a Bessel filter of sixth order and cutoff frequency of 62.5 Hz. The ADCs resolution is 12 bit and quantization noise was assumed to have a variance of 10 quantization steps and average 0. The sampling frequency was 800 kHz and the last sampled current value in the past controller period was used for control, to avoid calculation
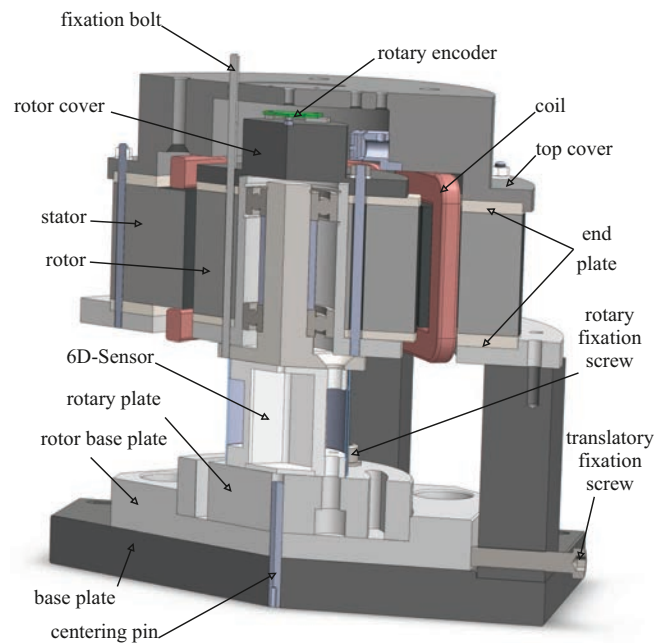

Figure 5. 3D plot of the test rig construction

time in the real-time-implementation. The controller frequency was 80 kHz. The power converters were modeled as ideal switches. All calculated controller parameters, as e.g. $L_{11,0}$ etc., were approximated with steps of $1°$.

V. TEST RIG

The test rig was constructed to enable static as well as dynamic measurements. In special the acting magnetic forces were of interest. In Fig. 5 a 3D-plot of the test rig is shown.

The rotor base plate can be moved with respect to the base plate to reach every rotor displacement u and v. The rotary plate carries a 6D-force sensor, which is connected to an axle with two ball bearings supporting the machines rotor. The permanent magnet for the rotary encoder is mounted on the rotor cover. The coils are mounted on the machines stator, which carries a top cover to ensure a safety operation and holding the stator part of the encoder.
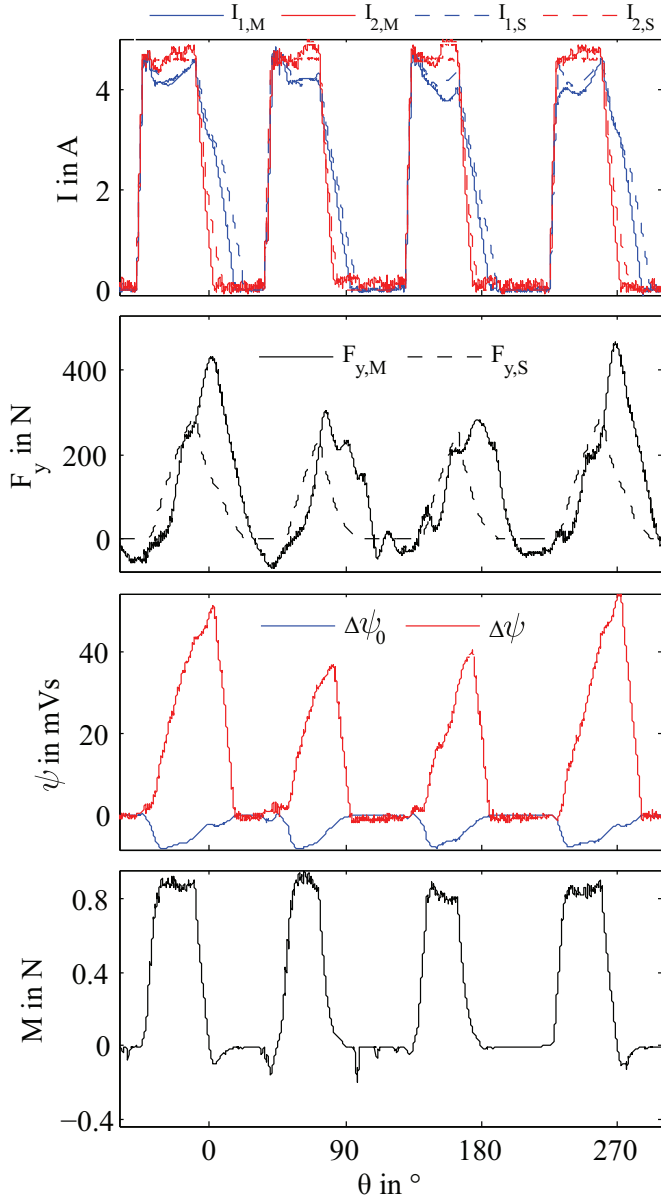
Figure 6. Comparison of measurement and simulation results in normal operation at 90 rad/s with a reference current of 4.5 A

Figure 7. Comparison of measurement and simulation results with unbalance force compensation at 90 rad/s with a reference current of 4.5 A

The controller was implemented on an ARM-Cortex-M4 DSP. The rotary encoder was operated in PWM-Mode with a frequency of 976.56 Hz. For that reason an angular observer was implemented to improve the measurement results. For this the angular verlocity was approximated with a least-squares based derivative estimator of third order and the actual angle approximated with the difference quotient.

The current was measured with a fluxgate sensor for the controller and a current probe for the measurement. The eight analog signals and the digital angle signal were measured with two mixed signal oscilloscopes, which were externally triggered by a PWM-output which was set to high when the reference angular velocity was reached.
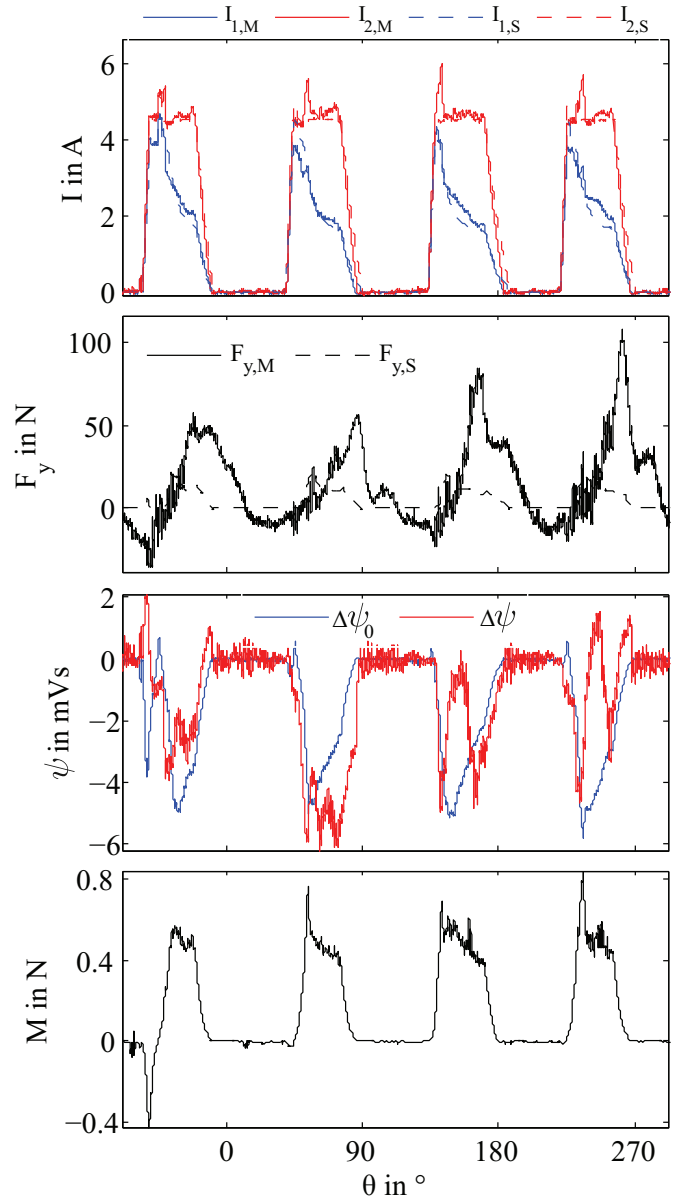
VI. MEASUREMENT RESULTS

To demonstrate the functionallity and to validate the simulation model, in this chapter a comparison to measurements is given. For this a constant angular velocity is assumed and the power supply is regulated to a link voltage of 30 V. The rotor is fixed at a translatory displacement of $u = 0$ mm and $v = 0.46$ mm. Furthermore only one phase will be considered, subsequent mutual coupling is eliminated. The measurement and the simulation was done once in normal operation with both currents having the same reference and once with the control scheme illustrated before.

The first bending mode of the rotor structure appears at 136 Hz and therefore the measured force was filtered with a second order IIR-notch filter with cutoff frequency 136 Hz.

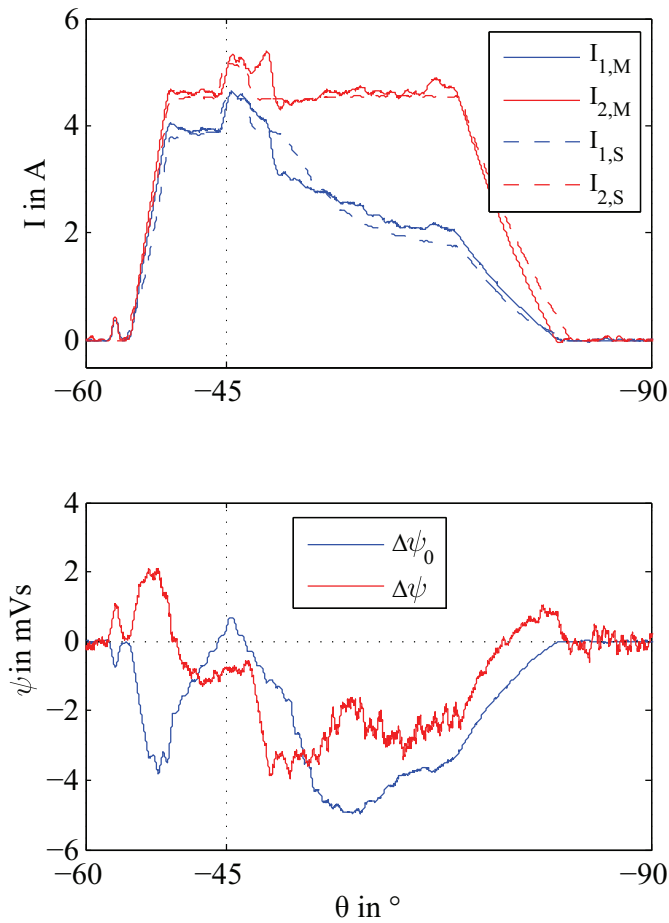Fig. 6 shows the comparison of measurement and simulation

Figure 8. Detailed plot of measurement and simulation results with unbalance force compensation at 90 rad/s with a reference current of 4.5 A

reference fluxdifference $\Delta\psi_0$ in the range of $\theta = 45°$ where the case distinction in (8) changes.

In contrast to the normal operation, the difference of the two fluxlinkages ist much smaller with force compensation. Nevertheless the result can be approved by using a PD-controller to minimize the control error in (7). Its worth noting, that also in the real-time-implementation machine characteristics from a 2D finite element analysis were used. Further improvement can be reached by using measured data.

VII. CONCLUSION AND OUTLOOK

In this paper a control method to compensate the unbalance forces of a SRM is presented. The key of this method is the separate control of the phase coils and adjust the fluxlinkages to achieve vanishing forces. Furthermore two fluxlinkage observers where discussed. Simulation results demonstrated the effectiveness of the controller in contrast to the method in [8], where major problems arised due to BEMF and thereby imprecise current control.

The validation was done at a special manufactured test rig. The results were in good agreement to the simulation results.

The real-time-implementation was done with simulated data only. Further optimization and better compensation can be reached by usage of measured values.

VIII. ACKNOWLEDGMENT

in normal operation at 90 rad/s with a reference current of 4.5 A. The turn-on and turn-off angles for the simulation were adapted to the measurement. The measured currents in the two coils are denoted as $I_{1,M}$ and $I_{2,M}$ and the simulated ones as $I_{1,S}$ and $I_{2,S}$. The same was done with unbalance force compensation, which is shown in Fig. 7. In both figures, the fluxlinkage difference was determined with (14) with simulated inductances but measured currents. The ploted torque is interpolated to the measured currents from the simulated characteristics.

In normal operation the maximum force is above 400 N while in Fig. 7 the force can be compensated to values about 100 N. Due to the large displacement the BEMF is very large for coil 1. Therefore in normal operation I_1 is below the reference current.

Due to the decreased current I_1 in Fig. 7 compared to normal operation the generated torque also decreases. This would be compensated by a superior controller to ensure to commanded torque.

In Fig. 8 the results of Fig. 7 are shown in more detail. One can see the good agreement of the simulated data to the measurements results. In the range of $\theta = 45°$ the current I_2 begins to rise above the reference value and I_1 reaches the reference current. This is due to the positive value of the

REFERENCES

[1] O.W. Andersen, "Compensation of Unbalanced Magnetic Forces by Distributed Parallel Circuits," *International Conference on Electrical Machines ICEM*, Krakow, Aug. 2004.

[2] J. Li, D. Choi and Y.H. Cho, "Compensation of Unbalanced Magnetic Force in Switched Reluctance Motor with Airgap Nonuniformity," *EPE Chapter Electric Drives Joint Symposium*, France, Jul. 2009.

[3] J. Li, D. Choi and Y.H. Cho, "Analysis of Rotor Eccentricity in Switched Reluctance Motor With Parallel Winding Using FEM," *IEEE Transactions on Magnetics*, Jul. 2009, Vol. 45, No. 6, pp. 2851-2854.

[4] H. Mansir, "Switched Reluctance Machine Having Unbalance Forces Compensation Coils," U.S. Patent 5 422 525, June 6, 1995.

[5] M. R. Tavakoli, H. Torkaman and E. Afjei, "Eccentricity faults compensation in SRMs by counterbalancing ampere turns in facing poles," *Power Electronics, Drive Systems and Technologies Conference (PEDSTC)*, 2013, pp. 66-71.

[6] H. Torkaman, E. Afjei and P. Yadegari, "Static, Dynamic, and Mixed Eccentricity Faults Diagnosis in Switched Reluctance Motors Using Transient Finite Element Method and Experiments," *IEEE Transactions on Magnetics*, 2012, Vol. 48, No. 8, pp. 2254-2264.

[7] J. Ji, Y. Sun, W. Zhao, X. Zhu and C. Song, "Calculation and remedial strategy of radial force of switched reluctance motors with eccentricity," *International Conference on Electrical Machines and Systems ICEMS*, 2008, pp. 3932-3935.

[8] T. Hinterdorfer, A. Schulz and H. Sima, "Force Prediction and Radial Force Compensation of a Switched Reluctance Motor," *39th Annual Conference on Industrial Electronics, IECON 2013*, pp. 2872-2877.